

Spatial-spectral Data Time Series Prediction Based on the Spatial Attention Iterative Model

Hongquan Chen¹, Shengwei Wang^{1*}, Yulin Guo², Wenjing Su¹, Shuohao Cui¹, Yurong Xu¹ and Zhiqiang Zhou¹

¹School of Computer Science and Engineering, Northwest Normal University, Lanzhou, 730000, China

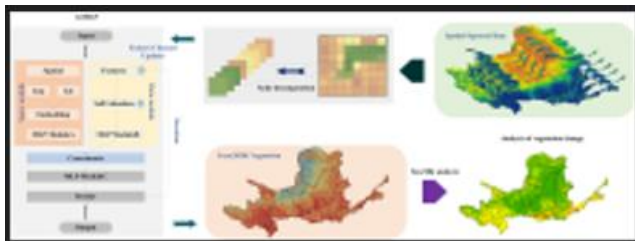
²Medical College of Northwest Minzu University, Lanzhou, 730000, China

Received: 10/01/2025, Accepted: 23/04/2025, Available online: 29/04/2025

*to whom all correspondence should be addressed: e-mail: wangsw@nwnu.edu.cn

<https://doi.org/10.30955/gnj.07250>

Graphical abstract



Abstract

In this study, a spatial attention iterative multi-layer perceptron model (SAi-MLP) is designed based on the temporal variation characterization of the pixels based on the Spatial-Spectra data. By extracting the spatial and temporal features of the data to predict the output, the output is used as a new feature channel input to iteratively predict the value of the next time node for ensuring the temporal continuity of the time series prediction. This study was carried out using the multi-temporal vegetation content of the Yellow River Basin as the base spatial-spectral dataset. The experimental results are as follows. (1) The performance metrics of SAi-MLP compared to other models are improved by about 2% in R2 and reduced by about 0.16%, 1.16%, and 1.35% in MSE, MAE, and RMSE, respectively. (2) SAi-MLP can spatially maintain spatial nearest neighbor information compared to MLP. (3) From 2000 to 2020, the vegetation cover of the Yellow River Basin showed an increasing trend. The highest average value of vegetation cover in 2018 and 2020 is 0.78, and the average value of vegetation cover in 2030 is 0.82, an increase of 0.22 compared with 2000.

Keyword : Iterative Time Series Prediction ; SAi-MLP ; Trend Analysis ; Yellow River Basin

1. Introduction

Spatial-spectral data have the characteristics of synchronous observation over a large area, strong timeliness, and the ability to objectively reflect the changes of terrain and surface features, which have become the main data source in environmental computing (Zheng *et al.* 2023). A large number of

prediction models have been proposed to realize high-precision time series prediction with spatial-spectral data (Alhnaity *et al.* 2021). The prediction models include traditional statistical models, machine learning models, deep learning models and hybrid models (Sundarapandi *et al.* 2024). Statistical models have limited prediction performance for abrupt changes in time series, while the application of machine learning and deep learning techniques address the problem of mutation prediction performance better. So far researchers have further utilized the use of combined prediction models to combine the advantages of each single prediction model (Yu *et al.* 2021). In this study, a self-iterative cascade prediction model is proposed, SAi-MLP, to predict the temporal changes of vegetation content as a feature of the spatial-spectral data.

Vegetation as a hub in terrestrial ecosystems is closely linked to ecological elements such as atmosphere, soil and hydrology, which plays a key role in maintaining and optimizing ecosystem services (Chen *et al.* 2021). Vegetation is the material basis for human survival and development (Luo *et al.* 2023), it also plays a pioneering role in energy flow and material cycling in ecosystems (Piao *et al.* 2011). Exploring vegetation changes by monitoring vegetation cover and growth conditions can reveal both the ecological environment evolution and its response mechanism. At the same time, it is of great significance for the in-depth understanding of the information transfer process of the ecosystem (Ding *et al.* 2016). In turn, it can provide theoretical basis for the governance and management of regional ecological environment (Wang h 2023c). Vegetation is generally calculated using both field observation and remote sensing image estimation (Gao *et al.* 2020). The maturity of remote sensing technology has enabled large-scale, high-precision remote sensing satellites to quickly and accurately reflect vegetation cover (Xiao *et al.* 2017).

Geographic Information System (GIS) has powerful spatial analysis and processing capabilities, so currently the method of combining remote sensing and GIS is mainly adopted (Song *et al.* 2015). Remote sensing image observation becomes the mainstream way to calculate

FVC, which acquires effective vegetation cover data through the combination between remote sensing data bands. Normalized vegetation index (NDVI) is characterized by the elimination of instrumental calibration and radiometric errors, as well as long time series and easy arithmetic (Wang *et al.* 2023b). The sensitivity of biological characteristics that change during vegetation growth largely attenuates the effects of atmosphere, soil background and vegetation type, so NDVI is widely used in the calculation of vegetation cover dynamics monitoring (Xie *et al.* 2023). The use of pixel dichotomous modeling to estimate FVC from NDVI content at different surface locations has been proposed for application (Liu *et al.* 2023).

Statistical analysis using available time-series data to infer trends in vegetation evolution is important for ecological monitoring. Studies have been conducted to discuss the characteristics of spatial and temporal changes in vegetation through multi-temporal vegetation trend analyses at large scales (Sun *et al.* 2021), but fewer methods have been used for prediction of long time series. The development of computer disciplines provides new methods for predicting the spatial evolutionary distribution of vegetation (Nelson *et al.* 2024), such as differential autoregressive moving average model (ARIMA) and Hurst index (Kang *et al.* 2021) applied in ecological time series prediction. This shift in disciplinary research perspectives reflects the transition from traditional geoscientific sample analysis to multidisciplinary fusion analysis. Machine learning theories have provided additional perspectives for environmental prediction meanwhile the use of LSTM and RNN to compute ecological factors to drive spatial evolution prediction techniques is relatively mature (Wang *et al.* 2023a).

However, how to parse the vegetation cover data can be better applied to the training of machine learning models must be further introduced to explore the interpretability. Vegetation cover has a large uncertainty in its estimation due to its spatial heterogeneity at horizontal and vertical scales, as well as differences in parameter factors and modeling methods (Xu *et al.* 2018). Quantitative assessment of spatial and temporal patterns of vegetation cover through gridded can more effectively explore the distribution of vegetation in spatial areas. Researchers used the grid scale for remote sensing data processing to sample the large-scale study area into small-scale grid cells. Each grid cell was used as data input for a machine learning model to fit the spatial and temporal evolution of ecological features (Zhang *et al.* 2020). There is information loss when resampling remotely sensed data into small-scale grid cells. At the same time, due to the use of grid cells as data drivers for machine learning methods, each grid cell is treated as independent of each other. Thereby, the geospatial interaction of information is severed and spatial proximity is ignored (Tobler *et al.* 1970). Images are essentially multi-channel matrices consisting of a number of pixels. Computer vision image processing algorithms were employed to transform 2D or

3D images into matrices for computation to establish connections between pixels (Li *et al.* 2023a). Therefore, in this study, the pixels of remote sensing images are used as the data driver of the machine learning method to avoid the information loss caused by scale transformation. In terms of maintaining the nearest neighbor effect in the image space, the latitude and longitude are considered to represent the distribution of each image in the space. The latitude and longitude are calculated for each pixel to extract its spatial domain information. In terms of analyzing the variation of vegetation content over multiple time periods, the self-attention mechanism is introduced to extract feature domain information. The self-attention mechanism is a special kind of attention mechanism that allows the model to process a sequence taking into account the relationship of each element of the sequence with all other elements. This mechanism can help the model to better interpret the contextual information in the sequence and to further process the sequence data more accurately (Li *et al.* 2023b).

Multi-Layer Perceptron (MLP) is generalized from Perceptron (PLA). Due to its multiple neuron layers, it is also called Deep Neural Network (DNN). MLP is a type of deep learning algorithm which consists of input, hidden and output layers (Murtagh. 1991). MLP uses back propagation to train the algorithm, which implements linear transformations through multiple hidden layers, thus being able to align the null-domain information with the feature-domain information output dimensions. It is widely used in ecological computing (Nunno *et al.* 2023). Previous researchers have used machine learning methods to predict future moment changes by targeting temporal data. Discrete temporal nodes are characterized by time domain discontinuity due to independent prediction tasks between inputs and outputs. For this reason in this study, the output sequence data is considered as a new sequence input to the model for iterative prediction to ensure the continuity of the time domain.

Therefore this study proposes a timing prediction self-iterative cascade model SAI-MLP based on the working mechanism of MLP. This model unites the spatial and temporal feature domains of the pixels, and predicts the future evolutionary distribution of changes in vegetation temporal sequence through multivariate feature fusion. Finally, the trend analysis is used to study the regional change trend. The overall design first uses pixels to quantitatively calculate the spatial variation of vegetation. Then the spatial module is constructed to extract the spatial near-neighbor information index of the pixels by latitude and longitude. Meanwhile, the data module based on self-attention mechanism is constructed to analyze the relationship between time series data. The features of the two modules are further spliced and fused into the prediction module for prediction. The results obtained from the prediction are iteratively incorporated into the model prediction as new features for a new round of evolutionary prediction. The Yellow River Basin was selected as the study area. The model performance

was evaluated by using multi-temporal FVC spatial-spectral data to validate the analysis and iteratively predicting the future vegetation change characteristics in the Yellow River Basin. The Theil-Sen Median (Sen) trend analysis and Mann-Kendall (MK) test were combined in the validation session to analyze the evolutionary trends.

Based on the work of previous researchers, this study predicts the future evolutionary distribution of vegetation temporal changes through multidisciplinary integration, and also investigates regional change trends through trend analysis. The purpose of this study is to analyze the evolutionary trend of vegetation in the temporal sequence. This study has the following significance: (1) The self-iterative cascade model SAI-MLP model is proposed for the temporal prediction of spatial-spectral data, which can extract the spatial information features of spatial-spectral data pixels, and at the same time extract the temporal features of the data based on the mechanism of self-attention. The model is able to achieve an iterative prediction function based on full

consideration of spatio-temporal data characteristics. (2) The modeling approach proposed in this study analyzes the vegetation evolution trend from the beginning to the end of the period in a spatial region by means of self-iterative trends, which provides support for regional environmental monitoring in the medium and long term.

2. Methods

2.1. Spatial Attention iterative Multi-Layer Perceptron Model

The SAI-MLP model consists of a cascade of three Multi-Layer Perceptron (MLP) modules (**Figure 1**). The data module learns the weight parameters on the temporal order of the pixels through a self-attentive mechanism. The spatial module converts sparse one-hot vectors into dense embedding vectors by splicing longitude features and latitude features of pixels. The embedding vectors and weighting parameters are then concatenated in the prediction module to obtain the predicted vegetation content values for the next time node.

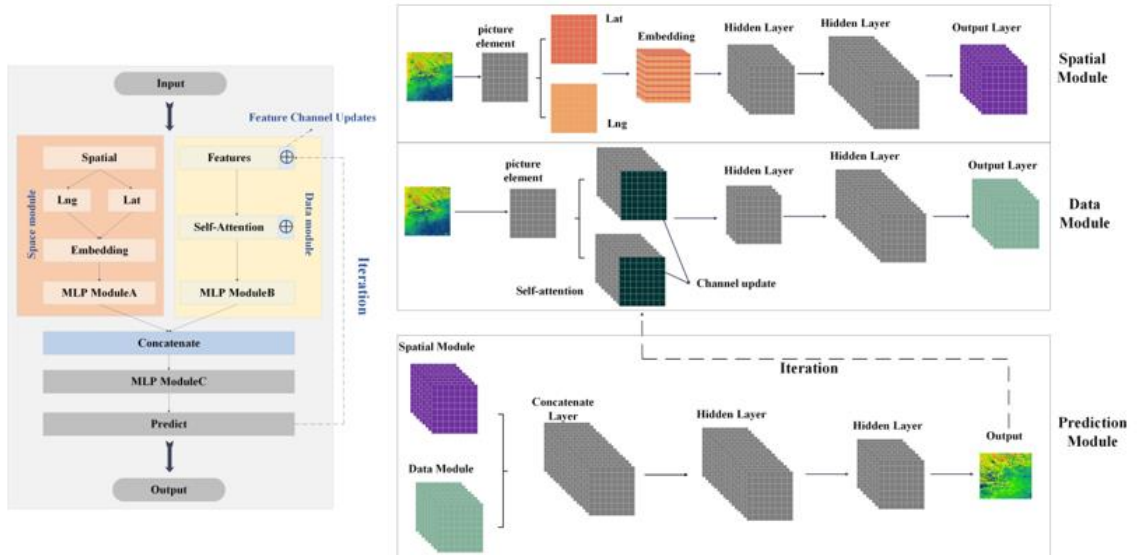


Figure 1. Architecture of SAI-MLP

2.1.1. Spatial Module

Longitude and latitude denote where each pixel is located in geographic space. We divide the study area into L and L' spatial segments according to longitude and latitude, respectively, and for a given S_{Lat} and S_{Lng} , take their indexes and convert them into solo heat vectors $V_{Lat} \in \mathbb{R}^{1 \times L}$, $V_{Lng} \in \mathbb{R}^{1 \times L'}$, which are used to denote the indexes of the pixels in terms of longitude and latitude. E_{Lat} and E_{Lng} are obtained by dimensionality reduction of V_{Lat} and V_{Lng} through Embedding layer, and the two layers are fused by one-dimensional stretching. The pixel latitude and longitude features are connected, then the connected data input into the MLP layer. The input data dimensions are changed by the MLP hidden layer. Finally the output is the matrix M_s of (R, M) .

2.1.2. Data Module

In 2017 Vaswani *et al.* proposed Multi-head Self-Attention Mechanism (Vaswani *et al.* 2017). It reflects the relationship between features through trainable Q, K, V parameters. The multi-head self-attention mechanism uses multiple heads employing the same computational approach given different parameters, which results in feature representation from multiple subspaces and is able to capture richer feature information (Li *et al.* 2023c). With the computation of Eq. (1), each head will get an output result of the correlation between features.

$$Attention(Q, K, V) = softmax(\frac{QK^T}{\sqrt{d_k}})V \quad (1)$$

Where Q, K, V are the parameter matrices and d_k is the latitude of the input sample set.

The data feature weights are computed into the MLP through the multi-head self-attention mechanism, the input data dimensions are changed through the hidden layer. As the result, the output is the matrix M_A of (S, M) .

2.1.3. Prediction Module

Two matrices M_S and M_A of the same dimension obtained from Spatial Module and Data Module are connected to obtain the matrix G :

$$G = \text{concat}[(M_S, M_A), \text{dim}=1] \quad (2)$$

The information matrix obtained by concatenating the spatial information matrix with the feature matrix is fed into the MLP and finally fed into the fully connected layer to predict the output through dimensional changes. The output is a new one-dimensional array of temporal features, populated into the original feature matrix, changing the original d_k in the Data Module to d_{k+1} . The number of self-attentive channels increases the number of channels with the increase of features, and the output through the MLP is the matrix M_A of (S, M) , which is connected to the Spatial Module to start the next round of prediction.

Algorithm: SAi-MLP algorithm	
Input:	$\{(Lat_n, Lng_n, F_n(\text{year})_{\text{year-begin of period}}^{\text{end of the period}})\}_{n=1}^{N_{\text{time}}}$, dataset of spatial-spectral Data Elements
Output:	$\{(Lat_n, Lng_n, F_n(\text{time}))_{n=1}^{N_{\text{time}}}\}$
1	repeat
2	if $E < \text{time do}$
3	$E = \text{end of the period}$
4	for $i \in N_{\text{spatial}} \text{ do}$
5	for $i \in N_{\text{data}} \text{ do}$
6	$EM = \text{Embedding}((Lat_n, Lng_n))$
7	$M_S = \text{MLP}(EM)$
8	$MH = \text{Multi-Head-Attention}(F_n(\text{year})_{\text{year-begin of period}}^{\text{end of the period}})$, Updating the feature field
9	$M_A = \text{MLP}(MH)$
10	$G = \text{Combine}[(M_S, M_A)]$
11	$F_n(E+1) = \text{MLP}(G)$
12	end of the period \leftarrow end of the period + 1
13	end
14	end
15	else return $\{F_n(E+1)\}_{n=1}^{N_{\text{time}}}$
16	end

2.2. Sen-MK Trend Analysis

The Theil-Sen Median (Sen) trend analysis is a robust nonparametric statistical method for trend calculation that reduces the effect of data outliers (Yu *et al.* 2023). Mann-Kendall (MK) is a nonparametric statistical test that has the advantage that it does not require the measurements to follow a normal distribution, nor does it require that the trend be linear, and is not affected by missing values and outliers, it has been very widely used in trend significance test for long time series data (Yuan *et al.* 2013). Usually Sen is combined with MK test for trend analysis of long time series data (Feng *et al.* 2022). The Sen slope is calculated as:

$$\beta = \text{Median}\left(\frac{X_j - X_i}{j - i} \mid \forall j > i\right) \quad (3)$$

Where Median () indicates that the median value is taken. If β is greater than 0, it indicates an increasing trend in vegetation cover and vice versa for a decreasing trend.

The Mann-Kendall statistical test formula is as follows. Define the standardized test statistic Z as:

$$Z = \begin{cases} \frac{S}{\sqrt{\text{Var}(S)}} & S > 0 \\ 0 & S = 0 \\ \frac{S+1}{\sqrt{\text{Var}(S)}} & S < 0 \end{cases} \quad (4)$$

where,

$$S = \sum_{i=1}^{n-1} \sum_{j=i+1}^n \text{sgn}(X_j - X_i) \quad (5)$$

$$\text{sgn}(X_j - X_i) = \begin{cases} 1 & X_j - X_i > 0 \\ 0 & X_j - X_i = 0 \\ -1 & X_j - X_i < 0 \end{cases} \quad (6)$$

$$\text{Var}(S) = \frac{n(n-1)(2n+5)}{18} \quad (7)$$

where n is the number of data in the sequence, X_j and X_i are the j th and i -th time series data, respectively.

2.3. Metrics of Evaluation

The study used the FVC data of the Yellow River Basin from 2000 to 2020 as the input $\mathcal{X} \in \mathbb{R}^{S \times 20}$ for the training and test sets, and the model predicted output as $\rho \in \mathbb{R}^{S \times 20}$. The FVC data of 2021 was used as the true value $\gamma \in \mathbb{R}^{S \times 1}$. The model performance was evaluated using MAE, MSE, RMSE and R2. The expressions are given below.

$$\text{MAE} = \frac{1}{S} \sum_{i=1}^S |\rho - \gamma| \quad (8)$$

$$\text{MSE} = \frac{1}{S} \sum_{i=1}^S (\rho - \gamma)^2 \quad (9)$$

$$\text{RMSE} = \sqrt{\frac{1}{S} \sum_{i=1}^S (\rho - \gamma)^2} \quad (10)$$

$$R2 = 1 - \frac{\sum_{i=1}^S (\gamma - \rho)^2}{\sum_{i=1}^S (\gamma - \bar{\gamma})^2} \quad (11)$$

where S denotes the sample size.

2.4. Experimental environment

The hardware and software devices used in this study are shown in **Table1**

Table1. Experimental platform configuration

Title	Versions
CPU	Intel i5-12450HX
GPU	NVIDIA GeForce RTX 4060Ti
Operating system	Windows11 64bit
CUDA	11.2
Programming language	Python 3.7
Experimental platforms	Pycharm, Matlab

3. Materials

The study used vegetation cover (FVC) as a time series predictive spatial-spectral data feature. Vegetation is often used as an important characterization factor in ecological restoration (Gong *et al.* 2021), ecological driver studies (Pan *et al.* 2023), and ecological change analyses (Yu *et al.* 2023) due to its unique ecological significance in spatial regions. The spatial area of the Yellow River Basin was selected for the study. In this study, the FVC air spectrum data were selected to evaluate and validate the model. After calculating the evolution pattern, the trend of vegetation evolution in the Yellow River Basin was analyzed to provide research value for environmental management.

3.1. Study Area

The Yellow River is the second largest river in China and the fifth largest river in the world. The river basin covers 102°02'~103°12'E longitude and 34°52'~35°48'N latitude (Figure 2). The Yellow River originates from the northern foot of Ba Yan Ka La Mountain on the Qinghai-Tibet Plateau, and flows through nine provinces (autonomous regions), namely Qinghai Province, Sichuan Province, Gansu Province, Ningxia Hui Autonomous Region, Inner Mongolia Autonomous Region, Shanxi Province, Shaanxi Province, Henan Province and Shandong Province. The total length of the basin is 5,464 km, with an area of 795,000 km². The Yellow River basin spans from west to east, connecting the Tibetan Plateau, the Loess Plateau, and the North China Plain, and eventually joins the Bohai Sea. The climate of the basin is continental, with semi-humid in the southeast, semi-arid in the center, and arid in the northwest, with large climatic differences, diverse landforms, and complex habitats (Wang *et al.* 2023d). With its large elevation drop and fragile ecosystem, it is both an important link covering and radiating the economic and social development of the eastern, central, and western provinces and regions, and one of the regions with the most intense human activities in the world. Maintaining the ecological health of the Yellow River plays a very important role in both national economic, social development and ecological security (Fan *et al.* 2020).

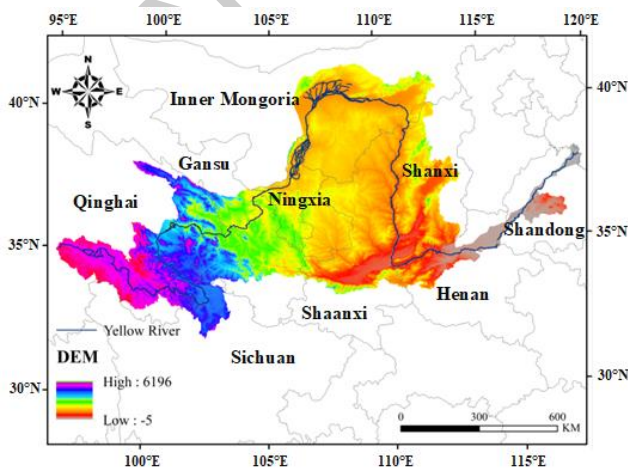


Figure 2. Study area

3.2. Materials sources

The remote sensing data acquired for the study were Landsat8 remote sensing images of the Yellow River Basin from 2000 to 2022. The dataset was obtained from USGS Earth Explorer by selecting the data of August when the vegetation cover grows luxuriantly. Firstly, Landsat8 multi-temporal remote sensing images were extracted by masking using the vector boundaries of the study area as the basic data source. Then the remote sensing data were processed by atmospheric correction, image stitching and image decoding. Finally, the hyperspectral data were filtered and smoothed by Savitzky-Golay method to reduce the interference of noise. The data sources are shown in Table 2.

Table 2. Data description

Data	Spatial resolution	Collection time	Data sources
Landsat 8	1km	2000-2023	USUG
DEM	1km	2022	RESDC

3.3. Research description

The flow of this study is shown in Figure 3. firstly, the remote sensing data collected from the study area from 2000 to 2022 were banded to calculate the vegetation cover (FVC). Secondly, the SAI-MLP spatio-temporal prediction model was designed based on the time series FVC data of pixels, and the performance indexes of different learning models and the SAI-MLP spatio-temporal prediction model were compared and verified to predict the future vegetation changes. Ablation experiments are designed to observe the performance and effect. Then the predicted results are used to analyze the trend of vegetation evolution in the Yellow River Basin in 2030 and construct the spatial pattern of vegetation evolution. Use Sen-MK to analyze the trend of vegetation change from 2000 to 2030.

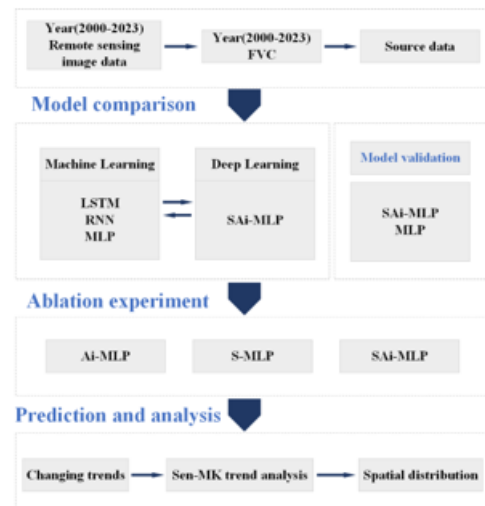


Figure 3. Research method

3.4. Calculation of feature

Vegetation cover was calculated by pixel dichotomous modeling. The principle of image-element dichotomous modeling allows the NDVI value of an pixel to be expressed in the form of a surface composition with a

vegetated portion versus a non-vegetated portion (Ma *et al.* 2023). The formula is as follows:

$$FVC = \frac{(NDVI - NDVI_{soil})}{(NDVI_{veg} - NDVI_{soil})} \quad (12)$$

Where FVC is the vegetation cover value and NDVI is the actual Normalized Difference Vegetation Index value. $NDVI_{soil}$ and $NDVI_{veg}$ represent NDVI values for bare soil and pure vegetation, respectively. In calculating the FVC, it is critical to determine the $NDVI_{soil}$ and $NDVI_{veg}$ values. Thresholds are typically determined using a confidence level based on the distribution of all NDVI values over the entire image. In this study, $NDVI_{soil}$ is the NDVI value of (0.05) for a cumulative frequency of 1% and $NDVI_{veg}$ is the NDVI value of (0.9) for a cumulative frequency of 99%.

NDVI is calculated using the formula:

$$NDVI = \frac{(NIR - Red)}{(NIR + Red)} \quad (13)$$

Where NIR denotes the near-infrared band, Red denotes the red light band.

The FVC content of each pixel from 2000 to 2022 was counted. Use it as a sample of time series data and divide the training set and test set for predictive model training in the ratio of 7:3.

4. Result

4.1. Characteristics of spatial variation

The spatial variation of vegetation cover in the Yellow River Basin from 2000 to 2022 was calculated using the pixel dichotomy method as shown in **Figure 4**. In 2000, the **Table 3**. FVC Data Statistics 2000-2022

Year	Mean	SD	V	Year	Mean	SD	V
2000	0.606	0.288	0.083	2012	0.756	0.244	0.06
2001	0.595	0.296	0.088	2013	0.744	0.26	0.068
2002	0.64	0.262	0.069	2014	0.711	0.26	0.067
2003	0.66	0.271	0.073	2015	0.678	0.286	0.082
2004	0.668	0.275	0.076	2016	0.727	0.254	0.064
2005	0.66	0.289	0.083	2017	0.72	0.263	0.069
2006	0.66	0.29	0.084	2018	0.78	0.23	0.053
2007	0.692	0.267	0.071	2019	0.75	0.245	0.06
2008	0.683	0.272	0.074	2020	0.78	0.249	0.062
2009	0.695	0.269	0.072	2021	0.605	0.288	0.083
2010	0.694	0.276	0.076	2022	0.595	0.296	0.088
2011	0.682	0.276	0.076	2012	0.756	0.244	0.06

4.2. Performance Comparison

4.2.1. Model Comparison

RNN, LSTM, and MLP are traditional models for processing time series data. RNN can process time series data of any length by using neurons with feedback (Zhang *et al.* 2023). RNN takes the hidden nodes of the $t - 1$ time slice as inputs to the current time slice at time slice t and thus has excellent performance on time series data. LSTM is a unique recurrent neural network (RNN) designed to learn

vegetation cover in the upstream and downstream areas of the Yellow River Basin is high. The middle reaches of the basin, including Gansu, Ningxia, and Inner Mongolia, have a low content of vegetation cover. In 2020, the vegetation cover in the upper and lower reaches of the Yellow River Basin remain stable, and it present a rich vegetation area in the whole basin. The vegetation cover in the middle reaches gradually improves. The direction of vegetation change shows an increasing trend from 34° N to 35° N, with the highest increasing content of 0.5.

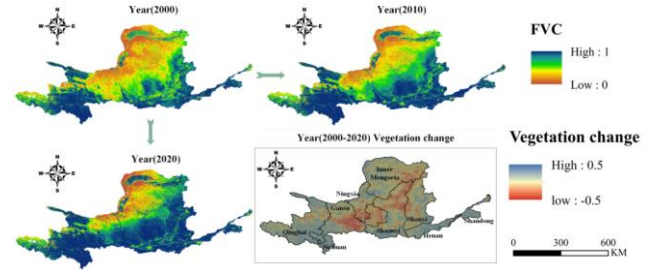


Figure 4. Changes in FVC content in the Yellow River Basin over a 20-year period (2000-2020)

The FVC content of each pixel was counted from 2000 to 2022, and the data statistics are shown in **Table 3**. Among them, the mean value of FVC in 2018 and 2020 is the highest in the same period, reaching 0.78. The variance is the smallest in 2018, which indicate that the differences in the content of each region of the Yellow River Basin in the period of vegetation abundance in 2018 are smaller than that in the other 21 years, and the overall performance present relatively stable.

long-term dependencies in sequence data. Compared to other RNN including GRU, LSTM achieves better performance by adding a gating mechanism to control the flow of information as well as state and cell updates (Hladek *et al.* 2019). MLP is a class of feed-forward artificial neural networks (Voukantsis *et al.* 2011), consisting of at least three layers of nodes, i.e., input layer, hidden layer, and output layer (Jamei *et al.* 2020). RNN, LSTM and MLP have a wide range of applications in environmental monitoring (Zhang *et al.* 2021).

The FVC pixel statistics data of the Yellow River Basin from 2000 to 2020 were divided into training and test sets according to 7:3, and the data of 2021 was taken as the real value. We use RNN, LSTM, MLP prediction model and SAI-MLP model to compare the performance of each index as shown in **Table 4**.

Table 4. Model Performance Evaluation

Model	MSE	MAE	R2	RMSE
LSTM	0.0031	0.0396	0.945	0.0559
RNN	0.004	0.0454	0.9445	0.0641
MLP	0.0058	0.058	0.9247	0.0762
SAI-MLP	0.0027	0.0367	0.964	0.0519

Comparing the results of various time series models on the test set, the SAI-MLP model improves about 2% on R2, reduces about 0.16% on MSE, 1.16% on MAE and 1.35% on RMSE as compared to RNN, LSTM and MLP models.

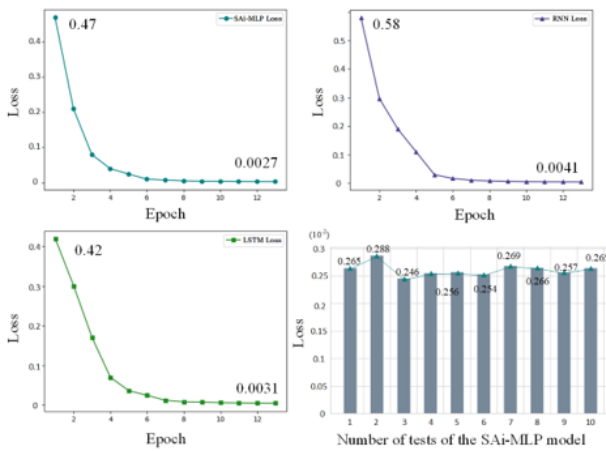


Figure 5. Model Loss Curve

Figure 5 shows the loss decreasing process of MSE for each type of model. The degree of convergence of all types of models is more satisfactory, and the loss of SAI-MLP model is smaller. Through several tests on the SAI-MLP model on time series data, the loss error is within 0.04%. SAI-MLP model shows better robustness.

4.2.2. Ablation experiments

The SAI-MLP model consists of three modules: the Spatial Module, the Data Module and the Predict Module. We analyze and further explore the performance impact of different parts on the baseline model by designing ablation experiments of different modules on the dataset. **Table 5** shows the S-MLP prediction model with the addition of Spatial Module, the Ai-MLP prediction model with the addition of Data Module, and the SAI-MLP prediction model with the fusion of the two Modules. Overall, the Ai-MLP, S-MLP and SAI-MLP outperform the basic temporal model in every performance. In addition, SAI-MLP also has an improvement over Ai-MLP and S-MLP, with an improvement of about 0.85% in R2, a reduction of about 0.1% in MSE, a reduction of about 0.38% in MAE, and a reduction of about 0.53% in RMSE. Therefore, SAI-MLP was selected as a predictive model for vegetation time series in the study area.

Table 5. Model Performance Evaluation

Model	MSE	MAE	R2	RMSE
Ai-MLP	0.0041	0.0454	0.9447	0.064
S-MLP	0.0031	0.0405	0.9576	0.0558
SAI-MLP	0.0027	0.0367	0.964	0.0519

4.2.3. Model validation

By comparing SAI-MLP with the models in terms of performance metrics, SAI-MLP outperforms the other models in all the metrics. Since deep learning focuses more on the data itself by analyzing the features between the data to reduce the loss of fit and thus predict the output. To explore the generalization ability of the model, data from 2000 to 2021 were used to predict the evolution of vegetation distribution in 2022, in parallel with the validation of the model using the actual spatial distribution of vegetation in the 2022 dataset. The model generalization results are shown in **Figure 6**.

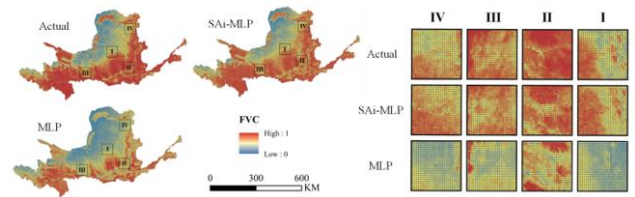


Figure 6. Validation Comparison

The 2022 vegetation cover data were used to validate the generalization performance of SAI-MLP against the base time series prediction model. The experimental results show that SAI-MLP outperforms the base model MLP in geospatial time series prediction, and the prediction results can better fit the real vegetation distribution. MLP can fit the vegetation cover in the northern and southern parts of the study area, but its prediction results in the central part of the study area are not satisfactory. MLP predicts the evolutionary trend of the vegetation through the information of the pixels, which focuses on the pixels themselves and is more inclined to discrete prediction. The predicted results show a discontinuous distribution of spatial patches, therefore the central zone where north meets south is not predicted to show a significant effect. The SAI-MLP model utilizes the latitude and longitude of the pixels with the surrounding pixels to maintain the continuity of spatial information, which can better show the continuity of spatial evolution than the MLP model. SAI-MLP adds the connection between the spatial patches on the discrete prediction of the MLP, so the prediction effect in the central part of the study area is significantly improved compared with the MLP. The prediction results obtained from the SAI-MLP model can better reflect the real vegetation distribution situation.

By comparing ASMLP with other models on the test set and validation set, ASMLP's prediction effect is better than other models. Therefore, the vegetation cover data from 2000 to 2022 were used as inputs, and the obtained outputs were used as inputs to the ASMLP model for new feature iterations to predict the spatial distribution of vegetation cover in the Yellow River Basin in 2030. The vegetation evolution characteristics of the Yellow River

Basin in the period from 2020 to 2030 were further analyzed.

4.3. Forecasting and analysis

The SAI-MLP model was used to predict the vegetation distribution in the Yellow River Basin in 2030 through the vegetation content data from 2000 to 2022 in the Yellow River Basin, and the output was iteratively predicted as a new characterization channel for the vegetation distribution in 2030 as shown in **Figure 7**. The 2030 vegetation abundance in the Yellow River Basin is still concentrated within the upstream and downstream segments, with Inner Mongolia, Ningxia and Gansu as vegetation fragile areas. The formation of this distribution pattern is related to regional characteristics. Ningxia and Inner Mongolia are located in Northwest China, as the more ecologically fragile regions in China (Zhao *et al.* 2017), dominated by wind-eroded landscapes with serious drought threats. Therefore, the early 21st century manifested as the main vegetation-poor area in the Yellow River Basin. After that, the government organized and implemented major national forestry projects such as the Three North Protective Forest, natural forest protection, and returning farmland to forest. By carrying out measures to protect vegetation such as mountain grazing ban, sand control, wetland protection, ecological restoration, and other related measures, the vegetation coverage has been continuously improved, thus enhancing the ecological environment of the watershed as a whole (Wu *et al.* 2021). Compared to 2023, the upper and lower reaches of the watershed remain solidly vegetated in 2030, with a decreasing area of low-vegetation in the middle reaches of the watershed. The overall upward trend in the vegetation content of the watershed in 2030 has a mean value of 0.72. Improvement of vulnerable vegetation areas shows an east to west path in the Inner Mongolia section and a south to north path in the Ningxia and Gansu sections. For the future ecological protection of the Yellow River Basin, Inner Mongolia, Ningxia and Gansu should be the main management areas. It is recommended to take advantage of the overall increase in vegetation content in the basin to reduce the inhibition caused by external factors such as man-made. At the same time, the implementation of green projects should continue to be promoted, and positive measures should be taken against wind erosion landforms, so that the ecology of the Yellow River Basin can be protected steadily in the end.

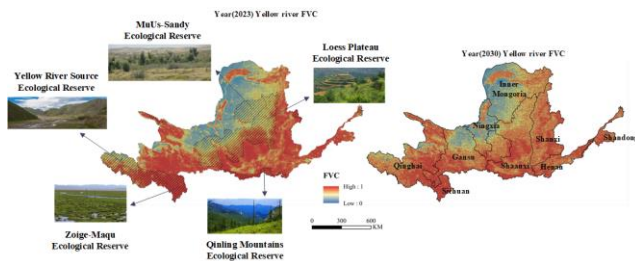


Figure 7. Vegetation evolution in the Yellow River Basin

Trend analysis of vegetation changes in the Yellow River Basin from 2000 to 2030 yield the following results (**Figure 8**), where positive values indicate improvement and negative values indicate degradation. The middle reaches of the Yellow River, as shown in the figure, have been significantly improved and are closely related to the green projects implemented. From 2000 to 2030, the vegetation changes in the basin show an upward trend, major upward areas in Ningxia, Inner Mongolia and Shanxi section. The direction trend of the vegetation gradually improves from south to north and from west to east. During the two decadal periods from 2000 to 2020, the vegetation content within the Gansu, Ningxia and Inner Mongolia sections showed an increasing and accelerating trend. In 2030, the vegetation vulnerability of the Yellow River Basin is still further improved, but the vegetation growth shows an increasing slow growth compared to the previous two decadal stages. The vegetation abundance in the study area has remained relatively stable in general, but there has been some degradation with the core areas of degradation being in the Shaanxi and Henan regions. The main areas of degradation are the developing cities of Xi'an and Zhengzhou, where urban expansion has caused major vegetation degradation.

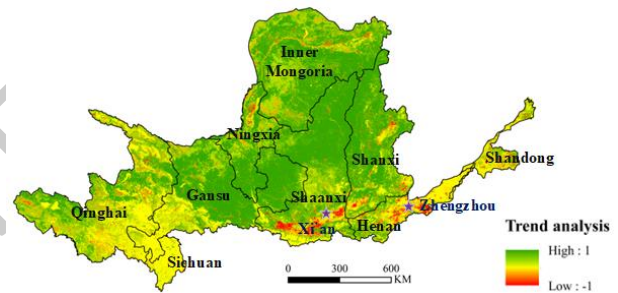


Figure 8. Trend analysis of vegetation Sen-MK from 2000 to 2030

5. Conclusion

In this paper, a spatial attention iterative multi-layer perceptron model (SAI-MLP) is constructed for temporal features to predict the evolution of spatial-spectral data. Spatial spectral data of vegetation content in the Yellow River Basin are used as the sample dataset for the model. The features are extracted by pixel fusion using the modeling method for multi-temporal spatial distribution of vegetation factors.

SAI-MLP implements spatio-temporal information extraction on sample data in the temporal and spatial domains. The spatial aspect embeds the geographic coordinates (latitude and longitude) of the pixels thus maintaining the proximity of the spatial data. The time domain aspect mines the temporal variations of features through the self-attention mechanism. The spatio-temporal information is then fused to predict the vegetation content at the next time node. In addition, the SAI-MLP model ensures temporal continuity in time-series prediction by adding the output value as an added channel to the model to iteratively predict the output. In this paper, the Yellow River Basin is taken as the study area, and then the main conclusions are as follows:

(1) By comparing SAi-MLP with other time series models, all performance indicators are improved. The SAi-MLP model has an improvement of about 2% in R2, a decrease of about 0.16% in MSE, a decrease of about 1.16% in MAE, and a decrease of about 1.35% in RMSE.

(2) Between 2000 and 2020, the vegetation in the Yellow River Basin shows a growing trend, with the highest growth content of 0.5. The mean value of vegetation cover in 2018 and 2020 is the highest in the same period, reaching 0.78. The variance is the smallest in 2018, and the overall performance is relatively stable.

(3) The vegetation of the Yellow River Basin in 2030 is gradually reduced by the area of low-vegetation regions within the Ningxia and Inner Mongolia sections. The mean value of FVC has been increased by 0.22 between 2000 and 2030, and by 0.04 between 2020 and 2030. The differences between the vegetation of the regions of the Yellow River Basin have a tendency to reduce.

(4) The trend of vegetation change from 2000 to 2030 is significantly improved in the middle reaches of the basin. There is obvious degradation of vegetation around the cities of Xi'an and Zhengzhou.

6. Discussion

In this paper, a self-iterative cascade model (SAi-MLP) is devised from the temporal variation of spatial-spectral features. The features of the next time node are predicted by extracting and fusing the spatial and temporal feature information of the data, followed by iterative prediction of the output as a new feature channel. The model ensures spatial near-neighbor information between the data in space and temporal continuity between the data in time by iteration, which has better applicability for spatial time-series prediction. By comparing and verifying with other time-series models, the proposed model performs well in terms of various performance indicators and prediction generalization ability. This can provide a better performance enhancement for the time-series prediction task. In future studies, we will also conduct follow-up research to explore the following two areas. (1) Explore the role of imaging factors in driving temporal changes in vegetation in anticipation of incorporating impact factor-driven principles into temporal prediction. (2) Further generalization capability enhancements to the self-iterative cascade model (SAi-MLP) allow it to be useful not only in spatial time-series prediction, but can be applied in more time-series iterative prediction scenarios.

Declarations

All authors have read, understood, and have complied as applicable with the statement on "Ethical responsibilities of Authors" as found in the Instructions for Authors

Funding

This research was supported by Gansu Key Research and Development Special Project for Ecological Civilization Construction under Grant No. 24YFFA062, and the National Natural Science

Foundation of China under Grant No. 32360434.

References

- Alhnaity, B., Kollias, S., Leontidis, G., Jiang, S.Y., Schamp, B., Pearson, S., 2021. An autoencoder wavelet based deep neural network with attention mechanism for multi-step prediction of plant growth. *J. Information Sciences*. 560,35-50.
- Chen, Y.Z., Feng, X.M., Tian, H.Q., Wu, X.T., Gao, Z., Feng, Y., Piao, S.L., Lv, N., Pan, N.Q., Fu, B.J., 2021. Accelerated increase in vegetation carbon sequestration in China after 2010: A turning point resulting from climate and human interaction. *J. Global Change Biology*. 27(22),5848-5864.
- Ding, Y.L., Zheng, X.M., Zhao, K., Xin, X.P., Liu, H.J., 2016. Quantifying the Impact of NDVIsoil Determination Methods and NDVIsoil Variability on the Estimation of Fractional Vegetation Cover in Northeast China. *J. Remote Sensing*. 8(1):29.
- Fan, J., Wang, Y.F., Wang, Y.X., 2020. High Quality Regional Development Research Based on Geographical Units: Discuss on the Difference in Development Conditions and Priorities of the Yellow River Basin Compared to the Yangtze River Basin. *J. Economic Geography*. 40(01),1-11.
- Feng, X.H., Zeng, Z.L., 2022. Natural Driving Forces of Vegetation Cover Characteristics and Change Trends in the Guangdong-Hong Kong-Macao Greater Bay Area. *J. Ecology and Environmental Sciences*. 31(09),1713-1724.
- Gao, L., Wang, X.F., Johnson, B.A., Tian, Q.J., Wang, Y., Verrelst, J., Mu, X.H., Gu, X.F., 2020. Remote sensing algorithms for estimation of fractional vegetation cover using pure vegetation index values: A review. *J. ISPRS Journal of Photogrammetry and Remote Sensing*. 159,364-377.
- Gong, S.H., Wang, S.J., Bai, X.Y., Luo, G.J., Wu, L.H., Chen, F., Qian, Q.H., Xiao, J.Y., Zeng, C., 2021. Response of the weathering carbon sink in terrestrial rocks to climate variables and ecological restoration in China. *J. Science of The Total Environment*. 750,141525.
- Hládek, D., Staš, J., Ondáš, S., 2019. Comparison of recurrent neural networks for Slovak punctuation restoration. *J. 2019 10th IEEE International Conference on Cognitive Infocommunications (CogInfoCom)*. 95-100.
- Jamei, M., Ahmadianfar, I., Chu, X.F., Yaseen, Z.M., 2020. Prediction of surface water total dissolved solids using hybridized wavelet-multigene genetic programming: New approach. *J. Journal of Hydrology*. 589,125335.
- Kang, Y., Guo, E.L., Wang, Y.F., Bao, Y.L., Na, R.M., 2021. Application of temperature vegetation dryness index for drought monitoring in Mongolian Plateau. *J. Chinese Journal of Applied Ecology* 32(07),2534-2544.
- Li, D.R., Sun, Z.Y., Jia, G., 2023a. Remote Sensing Image Analysis of Forest Land in Lushan Mountain and Its Surrounding Area Based on Mixed Pixel Decomposition. *J. Forest Inventory and Planning*. 48(04),1-12.
- Li, S.Y., Li, S.Y., Xu, R., Zhao, X.W., 2023b. Incomplete multi-view clustering algorithm based on self-attention fusion. *J. Journal of Computer Applications*. 1-10.
- Li, Y.Y., Liu, W.P., Huang, D., 2023c. Image Denoising Network Model Combined with Multi-head Attention Mechanism. *J. Computer Science*. 50(S2),326-333.
- Liu, L., Zheng, J.H., Guan, J.Y., Han, W.Q., Liu, Y.J., 2023. Grassland cover dynamics and their relationship with

- climatic factors in China from 1982 to 2021. *J. Science of The Total Environment*. 905,167067.
- Luo, Y.Z., Huang, Y.C., Wang, T., 2023. Spatial-temporal Variation Characteristics of Ecological Environment Quality and Their Driving Forces in Guangzhong Plain Urban Agglomeration, China. *J. Journal of Earth Sciences and Environment*. 1-14.
- Murtagh, F., 1991. Multilayer perceptrons for classification and regression. *J. Neurocomputing*. 2(5-6),183-197.
- Nelson, M., Rajendran, S., Khalaf, O.I., Hamam, H., 2024. Deep-learning-based intelligent neonatal seizure identification using spatial and spectral GNN optimized with the Aquila algorithm. *J. AIMS Mathematics*. 9(7):19645-19669.
- Nunno, F.D., Zhu, S.L., Ptak, M., Sojka, M., Granata, F., 2023. A stacked machine learning model for multi-step ahead prediction of lake surface water temperature. *J. Science of The Total Environment*. 890,164323.
- Pan, Z.Z., Gao, G.Y., Fu, B.J., 2022. Spatiotemporal changes and driving forces of ecosystem vulnerability in the Yangtze River Basin, China: Quantification using habitat-structure-function framework. *J. Science of The Total Environment*. 835,155494.
- Piao, S.L., Wang, X.H., Ciais, P., Zhu, B., 2011. Changes in satellite-derived vegetation growth trend in temperate and boreal Eurasia from 1982 to 2006. *J. 17(10)*,3228-3239.
- Song, N.P., Du, L.T., Wang, L., 2015. Vegetation dynamics over 2000-2012 and its driving factors in Yanchi County, Ningxia Province. *J. Acta Ecologica Sinica*. 22,7377-7386.
- Sundarapandi, A.M.S., Alotaibi, Y., Thanarajan, T., Rajendran, S., 2024. Archimedes optimisation algorithm quantum dilated convolutional neural network for road extraction in remote sensing images. *J. Heliyon*. 10(5):e26589.
- Sun, G.P., Liu, X.F., Wang, X.H., Li, S.S., 2021. Changes in vegetation coverage and its influencing factors across the Yellow River Basin during 2001-2020. *J. JOURNAL OF DESERT RESEARCH*. 41(4),205-212.
- Tobler, W.R., 1970. A Computer Movie Simulating Urban Growth in the Detroit Region. *J. Economic Geography*. 46, 234-240.
- Voukantsis, D., Karatzas, K., Kukkonen, J., Räsänen, T., Karppinen, A., Kolehmainen, M., 2011. Intercomparison of air quality data using principal component analysis, and forecasting of PM10 and PM2.5 concentrations using artificial neural networks, in Thessaloniki and Helsinki. *J. Science of The Total Environment*. 409,1266-1276.
- Wang, T., Tu, X.J., P. Singh, V., Chen, X.H., Lin, K.R., Zhou, Z.L., 2023a. Drought prediction: Insights from the fusion of LSTM and multi-source factors. *J. Science of The Total Environment*. 902,166361.
- Wang, T.X., Li, S., Zuo, C., Guo, X.H., Zhang, T.K., Zhang, X.J., 2023b. Spatio-temporal Evolution of Vegetation NDVI and Its Effect on Air Quality in Jingzhou City in Recent 20 Years. *J. Journal of Chinese Urban Forestry*.
- Wang, Y., Hao, L.N., Xu, Q., Li, J.Q., Chang, H., 2023c. Spatio-temporal variations of vegetation coverage and its geographical factors analysis on the Loess Plateau from 2001 to 2019. *J. Acta Ecologica Sinica*. 43(06),2397-2407.
- Wang, Z.J., Xu, M.Z., Hu, H.C., Zhang, X.P., 2023d. Characteristics of vegetation changes and their drivers in the Yellow River basin from 1982 to 2020. *J. Advances in Water Science*. 34(04),499-509.
- Wu, X., Zhang, Y.H., Wang, C.J., Fan, L.Q., Li, L., 2021. Analysis of temporal and spatial changes of vegetation coverage in Ningxia area based on MODIS. *J. Jiangsu Agricultural Sciences*. 49(02),204-208.
- Xiao, X., Li, J.Z., Han, B., Lu, C.P., Xue, B., 2017. Spatial-temporal characteristics of vegetation coverage and its correlation with urbanization in traditional industrial area of Northeastern China. *J. Ecological Science*. 36(06),71-77.
- Xie, J., Xie, B.G., Zhou, K.C., Li, J.H., Xiao, J.Y., Liu, C.C., Zhang, X.M., 2023. Evolution of bird habitat quality driving mechanisms and ecological network weights. *J. Global Ecology and Conservation*. 46,e02618.
- Xu, W.Y., Jin, X.B., Yang, X.H., Wang, Z.Q., Liu, J., Wang, D., Shan, W., Zhou, Y.K., 2018. The Estimation of Forest Vegetation Biomass in China in Spatial Grid. *J. Journal of Natural Resources*. 33(10),1725-1741.
- Yu, H.X., Zahidi, I., 2023. Spatial and temporal variation of vegetation cover in the main mining area of Qibaoshan Town, China: Potential impacts from mining damage, solid waste discharge and land reclamation. *J. Science of The Total Environment*. 859,160392.
- Yu, L., Du, B.W., Hu, X., Sun, L.L., Han, L.Z., Lv, W.F., 2021. Deep spatio-temporal graph convolutional network for traffic accident prediction. *J. Neurocomputing*. 423,135-147.
- Yu, T., Yang, P., Deng, X., Liu, S.H., Zhou, Y., 2023. Variation trend and comparative analysis of long-term vegetation cover in Mount Fanjing. *J. Bulletin of Surveying and Mapping*. (10),1-6.
- Yuan, L.H., Jiang, W.G., Shen, W.M., Liu, Y.H., Wang, W.J., Tao, L.L., 2013. The spatio-temporal variations of vegetation cover in the Yellow River Basin from 2000 to 2010. *J. Acta Ecologica Sinica*. 33(24),7798-7806.
- Zhang, R., He, X.L., Liu, J.L., Xiong, J.Y., 2023. VOC transport in an occupied residence: Measurements and predictions via deep learning. *J. Science of The Total Environment*. 892,164559.
- Zhang, B., Zou, G.J., Qin, D.M., Lu, Y.J., Jin, Y.P., Wang, H., 2021. A novel Encoder-Decoder model based on read-first LSTM for air pollutant prediction. *J. Science of The Total Environment*. 765,144507.
- Zhang, X.B., Luo, J., Shi, P.J., Zhou, L., 2020. Spatial-temporal evolution pattern and terrain gradient differentiation of ecosystem service value in Zhangye, Northwest China at the grid scale. *J. Chinese Journal of Applied Ecology*. 31(2):543-553.
- Zhao, Z.W., Zhang, L.P., Li, X., Wang, Y.X., Wang, S.L., 2017. Monitoring vegetation dynamics during the growing season in Ningxia based on MOD13Q1 data. *J. Progress in Geography*. 36(06),741-752.
- Zheng, Z.S., Wang, Z.H., Wang, Z.H., Lu, P., Huo, Z.J., Gao, M., 2023. Improved 3D-Octave convolutional hyperspectral image classification method. *J. Remote Sensing for Natural Resources*. 1-10.